Available online at www.sciencedirect.com
ScienceDirect
Medical Engineering & Physics 29 (2007) 708–717
Medical Engineering & Physics
www.elsevier.com/locate/medengphy

Haversian cortical bone model with many radial microcracks: An elastic analytic solution

A. Raeisi Najafi [a], A.R. Arshi [a,*], M.R. Eslami [b], S. Fariborz [b], M. Moeinzadeh [c]

[a] *Department of Medical Engineering, Amirkabir University of Technology, Tehran, Iran*
[b] *Department of Mechanical Engineering, Amirkabir University of Technology, Tehran, Iran*
[c] *Department of Industrial and Enterprise Systems Engineering, University of Illinois at Urbana-Champaign, USA*

Received 3 June 2005; received in revised form 23 July 2006; accepted 1 August 2006

Abstract

In this study, the fracture micromechanics of Haversian cortical bone has been considered. To this effect, a two-dimensional micromechanical fibre–ceramic matrix composite tissue materials model has been presented. The interstitial tissue was modeled as a matrix and the osteon was modeled as a fibre, followed by the application of linear elastic fracture mechanics theory. The solution for edge dislocations, in terms of Green's functions, was adopted to formulate a system of singular integral equations for the radial microcracks in the matrix in vicinity of the osteon. The problem was solved for various configurations and the corresponding stress intensity factors were computed. The results of this study indicated that the interaction between microcracks and an osteon was limited to vicinity of the osteon. Furthermore, the effect of microstructure morphology and heterogeneity on the fracture behavior has been established. The interactions between microcracks were also analyzed for various configurations. These selected configurations exhibited the effects of stress amplification and stress shielding.

Keywords: Haversian cortical bone; Microcrack interaction; Linear elastic fracture mechanics; Microstructure; Edge dislocation

1. Introduction

Bone undergoes microdamage in the form of microcracks due to fatigue and cyclic loading [1–3]. The microcracks can coalescence causing a reduction in the mechanical properties of the bone [4,5]. The weakness caused by microcracks has been accepted as a primary assumption in the study of mechanical properties of this tissue [5–7]. This will increase the possibility of fracture [8–10]. The relationship between the microcracks and the parameters governing fracture, e.g. those associated with toughness, has not as yet been fully understood and analyzed [11–13].

Formation and growth of microcracks are related to the bone microstructure [1,14]. The human Haversian cortical bone has been considered as a composite material and modeled as fibre–ceramic matrix in microstructural studies [15–17]. Osteons are considered as fibres and interstitial tissue as matrix in this composite material. The interface between the osteons and interstitial tissue is a third type of tissue forming the cement line.

Fracture phenomena in Haversian cortical bone are primarily affected by the morphology and heterogeneity of the microstructure [12–14,18]. However, variations in these parameters caused by the aging process can make the problem rather more complicated [12,19,20]. For example, the aging process increases the differences in the mechanical properties of osteons and interstitial tissue [19]. This has a profound effect upon the fracture behavior of bone [12,13]. It is thus necessary to enhance the understanding of the mechanisms governing fracture in Haversian cortical bone [18].

In this study, linear elastic fracture mechanics (LEFM) theory was adopted for the analysis of fracture in composite fibre–ceramic matrix materials [21]. This theory has also been used in determination of the bone resistance to fracture [22–24]. However, only a limited number of studies have considered fracture micromechanics in the Haversian cortical

* Corresponding author. Tel.: +98 21 88883772.
E-mail address: arshi@aut.ac.ir (A.R. Arshi).

1350-4533/$ – see front matter © 2006 IPEM. Published by Elsevier Ltd. All rights reserved.
doi:10.1016/j.medengphy.2006.08.001

bone [13,25–27]. Amongst such investigations, Lakes et al. have reported that the fracture behavior of microcracks with lengths of 250–500 μm in Haversian cortical bone can not be predicted by LEFM of a uniform material [25]. Furthermore, Martin and Burr have reported microcrack growth-arrest by the cement line [27]. Guo et al. have reported on the osteonal effect on a microcrack that was oriented perpendicularly to the external load [13]. However, a detailed description of the relationship between microcracks and fracture behavior has not as yet been provided. To understand this relation, it is necessary to begin by formulating a sufficiently encompassing description of microcrack governing micromechanics, accompanied by the description of the interaction between existing microcracks.

The objectives of the current study have been to provide a realistically simple model of Haversian cortical bone microstructure, so as to obtain a clearer description of the rules governing the mutual interaction amongst microcracks assuming LEFM theory. Furthermore, interaction between an osteon and radial microcracks was studied to establish the susceptibility of fracture behavior to microstructure.

2. Methods

The assumption of plane strain conditions and linear elastic fracture mechanics in a two-dimensional model of the bone could be justified by the similarities between Haversian cortical bone and the composite fibre–ceramic matrix materials. The osteons were represented as fibres and the interstitial tissue was considered as a matrix and the cement line was excluded in this model. All the tissues were assumed homogenous. Furthermore, the osteonal interaction was ignored by considering a single osteon. Exclusion of the Haversian channel structure, on the other hand, leads to the single osteon being represented by a solid cylinder.

The model consists of a single osteon with the radius $R_0 = 100$ μm [17], and constants of K_2 and G_2 situated within a matrix resembling the interstitial tissue with constants K_1 and G_1, as shown in Fig. 1, where G_i are the shear moduli and K_i, with respect to Poisson's ratio (ν_i) in plane strain condition, are computed as $K_i = 3–4\nu_i$. Here (n) radial microcracks, each having a length $2L_i$, where L_i is assumed to be 50–150 μm [9], were situated within the interstitial tissue. A uniform tensile load of $\sigma_0 = 10$ MPa was applied to the model at the infinity [16]. The interface between the osteon and the interstitial tissue was also assumed to be a perfectly bonding.

Mechanical properties of bone constituents are greatly affected by such factors as bone type and anatomical location. The average elastic moduli in human diaphyseal femoral bone, for example, are found to be 19.3 ± 5.4 GPa in osteonal and 21.2 ± 5.3 GPa in interstitial lamellae [28]. In the neck, the average moduli are 15.8 ± 5.3 GPa in osteonal, 17.5 ± 5.3 GPa in interstitial lamellae [28]. Table 1 shows the various mechanical properties of individual constituents in the model.

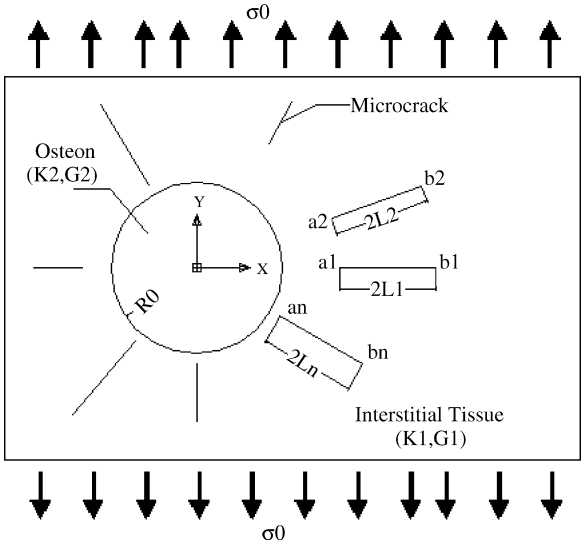

Fig. 1. Osteon-interstitial tissue model.

It was thus possible to solve the problem as a superposition of two distinct problems. In the first problem, an elastic osteon situated within an infinite elastic plane, similar to interstitial tissue, and without any microcracks was considered. This problem was solved for an external load of σ_0.

The second problem described stress disturbance due to microcracks in the interstitial tissue. Here, the external loads were limited to the microcrack surface tractions. The external loads were equal in magnitude and opposite in sign to the obtained stress in the presumed location of microcracks as described by the first problem. It should, however, be noted that formulation of stress equations for individual microcracks does entail the effects of other microcracks. It is apparent that the second problem contains a singularity.

2.1. Solutions of equations of elasticity, in polar coordinates

Solution of the first problem for a uniaxial tension at infinity is as follow [29]:

$$p_{rr} = \sigma_0 \left[\cos^2\theta - 2G_1 \left(\frac{A}{r^2} + \left(-\frac{3B}{r^4} + \frac{2C}{r^2}\right) \cos 2\theta\right)\right] \tag{1a}$$

Table 1
Mechanical properties of model constituents

	Effective elastic modulus (GPa)		Effective shear modulus (GPa)	
	Osteon fibre[a] (E_2)	Interstitial tissue[a] (E_1)	Osteon fibre[a] (G_2)	Interstitial tissue[a] (G_1)
Soft osteon	19	21	7.31	8.08
Stiff osteon	19	16	7.31	6.15

[a] Poisson's ratio $\nu_1 = \nu_2 = 0.3$.

$$p_{\theta\theta} = \sigma_0 \left[\sin^2\theta + 2G_1\left(\frac{A}{r^2} - \frac{3B}{r^4}\cos 2\theta\right)\right] \tag{1b}$$

$$p_{r\theta} = \sigma_0 \left[-\frac{\sin 2\theta}{2} + 2G_1\left(\frac{3B}{r^4} - \frac{C}{r^2}\right)\sin 2\theta\right] \tag{1c}$$

where

$$A = \frac{R_0^2}{4G_1}\frac{(K_2-1)-(K_1-1)\mathrm{GR}}{2\mathrm{GR}+(K_2-1)} \tag{2a}$$

$$B = \frac{R_0^4}{4G_1}\frac{1-\mathrm{GR}}{1+K_1\mathrm{GR}} \tag{2b}$$

$$C = \frac{R_0^2}{2G_1}\frac{1-\mathrm{GR}}{1+K_1\mathrm{GR}} \tag{2c}$$

$$\mathrm{GR} = \frac{G_2}{G_1} \tag{2d}$$

Here, r and θ are polar coordinates where r is measured from the center of the osteon and θ is measured with respect to the load direction. In providing a solution to the first problem, the shear and normal stress (p_{t_i} and p_{n_i}) at t, a point on the location of ith imaginary microcrack, had to be computed.

2.2. Integral equations

To solve the second problem, however, dislocation solution [30] could be used. The dislocations Burgers vectors (b_t and b_n) were placed along and perpendicular to the microcracks direction, respectively. The shear stress and normal stress values in the microcrack location were equal in magnitude but with opposing signs to that of the first problem [21]. The dislocation density (B_t and B_n) at ξ, a point on the microcrack, could thus be defined as

$$\delta b_t = B_t(\xi)\,\mathrm{d}\xi, \quad \xi \in L_i \tag{3a}$$

$$\delta b_n = B_n(\xi)\,\mathrm{d}\xi, \quad \xi \in L_i, \quad i = 1, 2, \ldots, n \tag{3b}$$

Here the microcrack opening displacement and the dislocation density were related by Eq. (4) as

$$u_t(\xi)|_0 - u_t(\xi)|_{2\pi} = -\int_{a_i}^{\xi} B_t(\xi)\,\mathrm{d}s, \quad i = 1, 2, \ldots, n \tag{4a}$$

$$u_n(\xi)|_0 - u_n(\xi)|_{2\pi} = -\int_{a_i}^{\xi} B_n(\xi)\,\mathrm{d}s, \quad a_i \le \xi \le b_i \tag{4b}$$

Since the microcrack tip opening displacements were equal to zero, Eq. (5) would have implied:

$$\int_{a_i}^{b_i} B_t(\xi)\,\mathrm{d}s = 0 \tag{5a}$$

$$\int_{a_i}^{b_i} B_n(\xi)\,\mathrm{d}s = 0, \quad i = 1, 2, \ldots, n \tag{5b}$$

Now, if it is assumed that b_t and b_n are continually distributed over the microcracks, the shear and normal stresses could be formulated as

$$\sigma_{t_i}(t) = \sum_{j=1}^{n}\int_{-1}^{1}[k_{t_1}(s,t)b_t(s) + k_{t_2}(s,t)b_n(s)]\,\mathrm{d}s \tag{6a}$$

$$\sigma_{n_i}(t) = \sum_{j=1}^{n}\int_{-1}^{1}[k_{n_1}(s,t)b_t(s) + k_{n_2}(s,t)b_n(s)]\,\mathrm{d}s,$$
$$i, j = 1, 2, \ldots, n \tag{6b}$$

The computation method for k_{t_1}, k_{t_2}, k_{n_1}, and k_{n_2} are presented in Appendix A. Furthermore, variables s and t in Eq. (6) are defined as

$$x_i = x_{i_\mathrm{m}} + (L_i\cos\alpha_i)t \tag{7a}$$

$$y_i = y_{i_\mathrm{m}} + (L_i\sin\alpha_i)t \tag{7b}$$

$$\xi_i = x_{i_\mathrm{m}} + (L_i\cos\alpha_i)s \tag{7c}$$

$$\eta_i = y_{i_\mathrm{m}} + (L_i\sin\alpha_i)s \tag{7d}$$

In Eq. (7), the x_{i_m} and y_{i_m} represent the coordinates of the ith microcrack center and α_i is the ith microcrack direction with respect to the horizontal axis.

After separating the singular part from dislocation density, B_t and B_n with respect to the unknown functions $f_t(s)$ and $f_n(s)$ could be defined as

$$B_t(s) = \frac{f_t(s)}{\sqrt{1-s^2}} \tag{8a}$$

$$B_n(s) = \frac{f_n(s)}{\sqrt{1-s^2}} \tag{8b}$$

Substituting Eq. (8) in Eqs. (5) and (6):

$$\sigma_{t_i}(t) = \sum_{j=1}^{n}\int_{-1}^{1}\left[k_{t_1}(s,t)\frac{f_t(s)}{\sqrt{1-s^2}} + k_{t_2}(s,t)\frac{f_n(s)}{\sqrt{1-s^2}}\right]\mathrm{d}s \tag{9a}$$

$$\sigma_{n_i}(t) = \sum_{j=1}^{n}\int_{-1}^{1}[k_{n_1}(s,t)\frac{f_t(s)}{\sqrt{1-s^2}} + k_{n_2}(s,t)\frac{f_n(s)}{\sqrt{1-s^2}}]\,\mathrm{d}s,$$
$$i, j = 1, 2, \ldots, n \tag{9b}$$

$$\int_{-1}^{1}\frac{f_t(s)}{\sqrt{1-s^2}}\,\mathrm{d}s = 0 \tag{10a}$$

$$\int_{-1}^{1}\frac{f_n(s)}{\sqrt{1-s^2}}\,\mathrm{d}s = 0 \tag{10b}$$

The unknown functions $f_t(s)$ and $f_n(s)$ could thus be determined by substituting, equal in magnitude and opposite in sign, stress values from the first problem to that of the second:

$$\sigma_{t_i}(t) = -p_{t_i}(t) \tag{11a}$$

$$\sigma_{n_i}(t) = -p_{n_i}(t) \tag{11b}$$

2.3. Stress intensity factors

The stress intensity factor (SIF) in the microcrack tips could be obtained once the functions $f_t(s)$ and $f_n(s)$ were determined:

$$k_{\mathrm{I}}|_{s=\pm1} = \pm\frac{2G_1}{k+1}\sqrt{L_i}\, f_n(\pm1) \tag{12a}$$

$$k_{\mathrm{II}}|_{s=\pm1} = \pm\frac{2G_1}{k+1}\sqrt{L_i}\, f_t(\pm1) \tag{12b}$$

The derivation of expression (12) is provided in Appendix B.

3. Results

A radial microcrack, as shown in Fig. 2, with a constant length perpendicular to the external loading was considered in the interstitial tissue. The mode I stress intensity factor (K_{I}) variation in the microcrack tips is shown for this condition with respect to the microcrack distance (d) to the osteon in Fig. 2(b). Here, the reduction of d was found to be accompanied by an increase in (K_{I}), when the osteon was considered to be softer than the interstitial tissue (GR = 0.5). When the osteon was stiffer than the interstitial tissue (GR = 2.0), the SIF was found to decrease as d was reduced. The results have shown the interaction between the osteon and microcracks was limited to the vicinity of the osteon.

To analyze the microcrack interaction, two microcracks with a distance (d) apart, were considered as indicated by Fig. 3. The existence of another microcrack increased the stress intensity factor (SIF) at crack tips as shown in Fig. 3(b) and (c). The figure shows the stress amplification in the SIF. This interaction was significantly reduced as d was increased. The reduction, however, approached a limit set by the value of the SIF for a single microcrack.

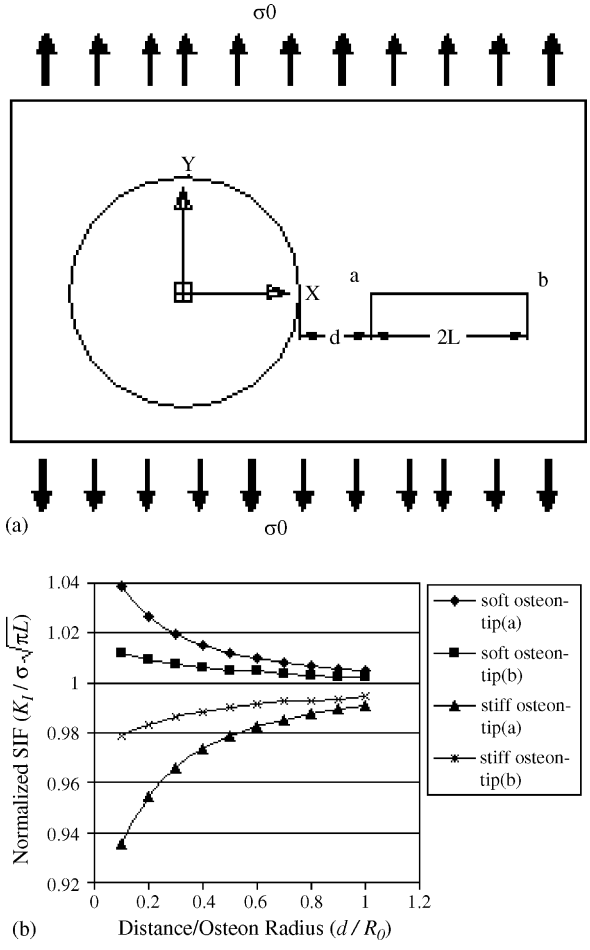

Fig. 2. (a) Model and (b) the normalized SIF of microcrack tips vs. the normalized distance (d/R_0) from the osteon. Interaction between osteon and the microcrack is limited to the vicinity of the osteon.

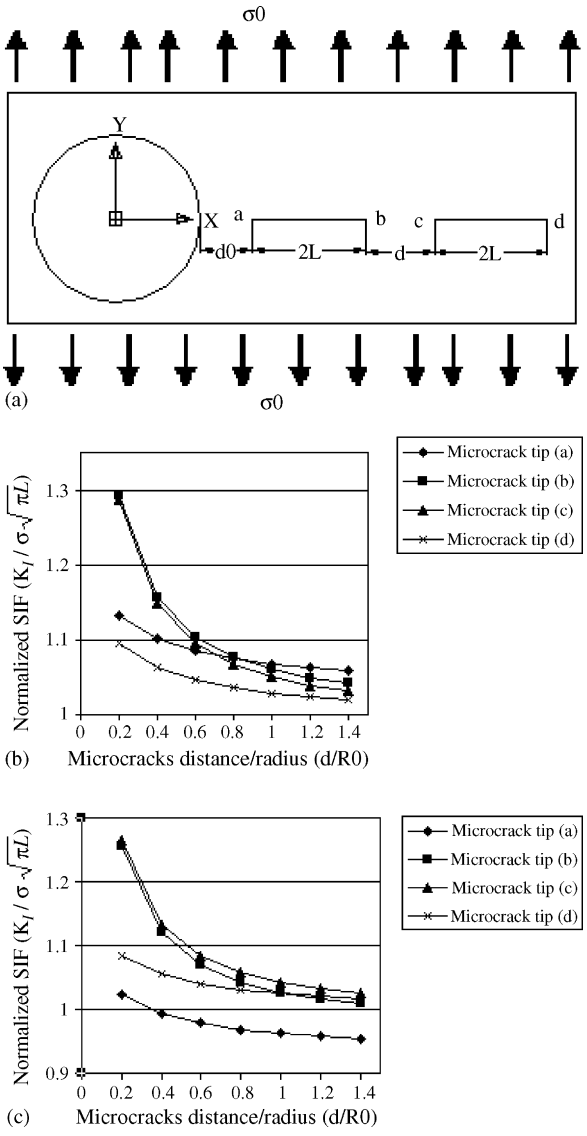

Fig. 3. The normalized SIF of microcrack tips vs. the normalized distance between two microcracks (d/R_0). Figure indicates "stress amplification" effect. (a) Model; (b) soft osteon (GR = 0.5); (c) stiff osteon (GR = 2.0).

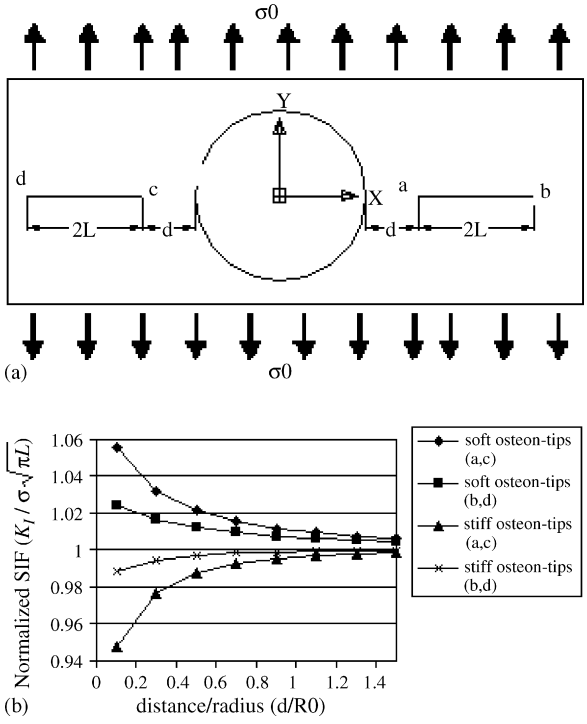

Fig. 4. (a) Model and (b) the normalized SIF of microcrack tips vs. the normalized distance (d/R_0) from the osteon.

Microcrack interaction was also found to be negligible if the microcracks were located symmetrically on both sides of the osteon as shown in Fig. 4. Here, the SIF changes accompanying an increase in d were found to be similar to that observed in Fig. 2. In effect, the osteon was found to exhibit an overriding influence when the distance between the microcracks was greater than the osteonal diameter.

The SIF variation in modes I and II (K_I and K_{II}), when the radial microcrack angle (α) changed with respect to horizontal axis, is shown in Fig. 5. The figure indicates that $K_I(a)$ and $K_I(b)$ were reduced as the angle (α) was increased. Here, the SIF in mode II was found to rise as (α) was increased to 45°. A reduction of SIF was, however, observed as the angle was further increased.

The effect of the two microcracks upon one another when there was an angle (α) between them is shown in Fig. 6. As can be seen, the first microcrack was assumed to be located along the horizontal axis. The second microcrack was orientated to make an angle (α) to the first. In such a situation, the $K_I(a)$ and $K_I(b)$ associated with the first microcrack tips were found to be reduced by the existence of the second microcrack. The interaction of microcracks was an indication of stress shielding. This effect, however, was reduced as the angle (α) increased. This reduction approached a limit set by the value of SIF for a single microcrack.

The existence of a secondary microcrack could have either a rising effect on SIF (stress amplification) or a reducing effect (stress shielding) as shown in Figs. 3 and 6. To study these phenomena, a number of microcracks were added to the model as shown in Fig. 7. Table 2 represents the results of this

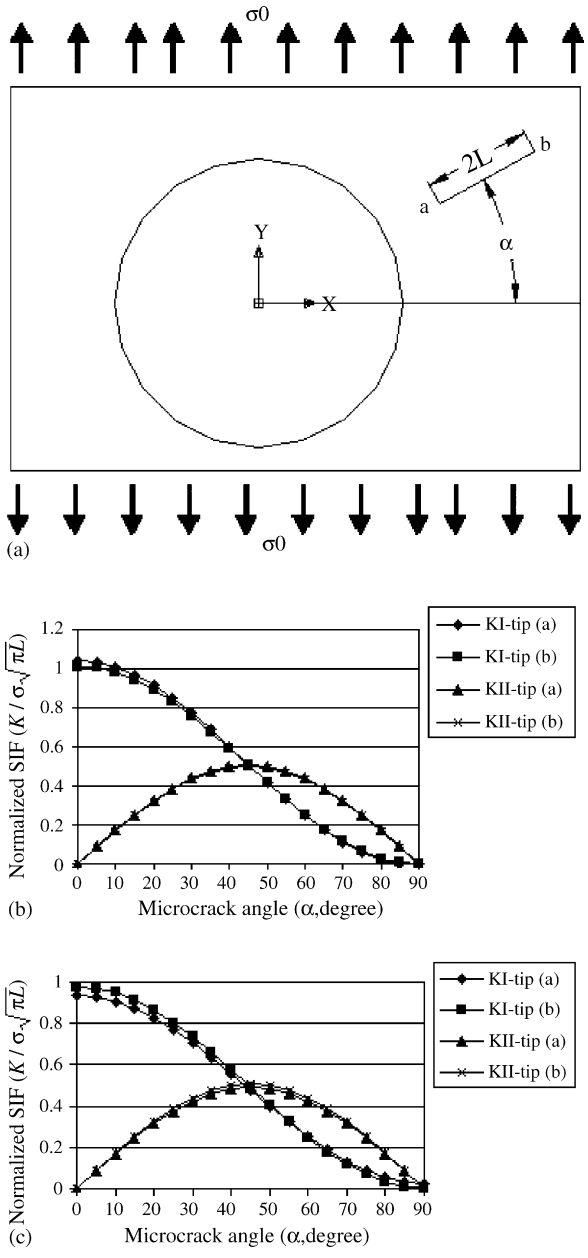

Fig. 5. The normalized SIF of microcrack tips vs. microcrack angle (α). (a) Model; (b) soft osteon (GR = 0.5); (c) stiff osteon (GR = 2.0).

Table 2
Stress amplification effect

	Number of microcracks				
	2	3	4	5	6
GR = 0.9					
K_I $(a)/K_{I0}$ (a)	1.0879	1.1022	1.1186	1.1328	1.1442
K_I $(b)/K_{I0}$ (b)	1.2748	1.3369	1.3831	1.3920	1.383
GR = 1.19					
K_I $(a)/K_{I0}$ (a)	1.0925	1.1074	1.1245	1.1393	1.1511
K_I $(b)/K_{I0}$ (b)	1.2784	1.3413	1.3879	1.3965	1.3851

K_{10} is SIF at the tip of primary microcrack (1) when other microcracks were absent.

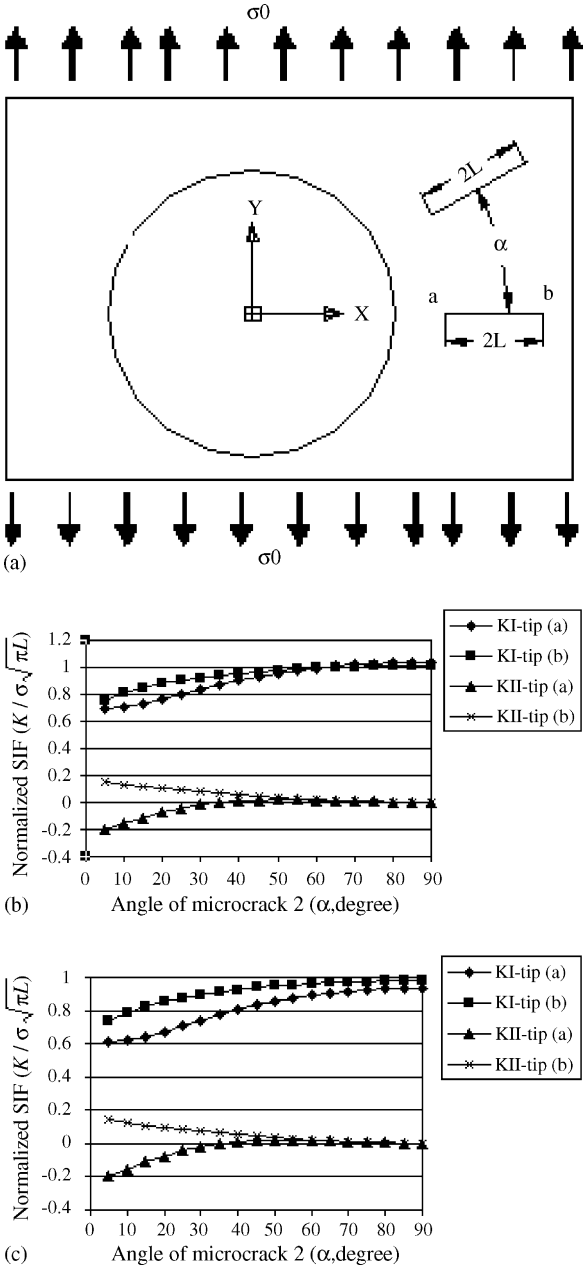

Fig. 6. The normalized SIF of microcrack tips vs. the angle (α) between two microcracks. Figure indicates the "stress shielding" effect. (a) Model; (b) soft osteon (GR = 0.5); (c) stiff osteon (GR = 2.0).

expansion. Here, the SIF associated with the first microcrack was observed to increase as number of added microcracks was raised. This increase in SIF is an example of stress amplification.

Analysis of the model was further progressed by retracting all secondary microcracks and repeating the tests by adding a number of microcracks to the primary microcrack as shown in Fig. 8. Table 3 represents the results. As the number of added microcracks increased, the SIF value for the primary microcrack was reduced. This could be influenced by the stress shielding phenomena.

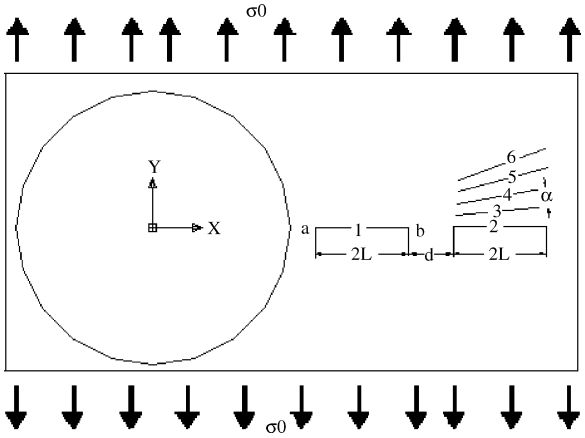

Fig. 7. Microcrack configuration for the "stress amplification" effect.

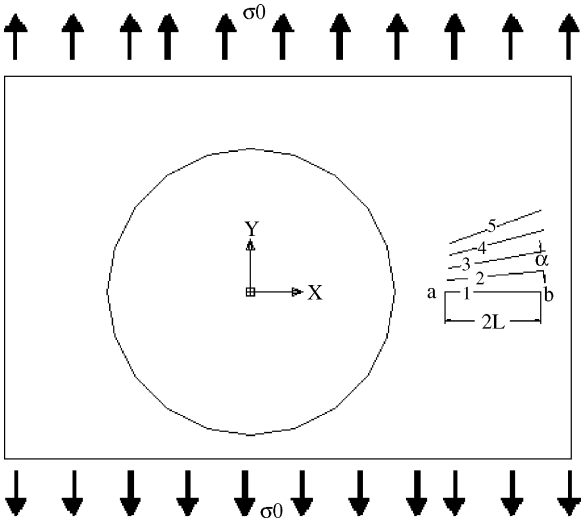

Fig. 8. Microcrack configuration for the "stress shielding" effect.

Table 3
Stress shielding effect

	Number of microcracks			
	2	3	4	5
GR = 0.9				
K_I $(a)/K_{I0}$ (a)	0.6561	0.6459	0.6958	0.5360
K_I $(b)/K_{I0}$ (b)	0.7082	0.7021	0.7484	0.6405
GR = 1.19				
K_I $(a)/K_{I0}$ (a)	0.6483	0.6435	0.5802	0.5255
K_I $(b)/K_{I0}$ (b)	0.7097	0.7035	0.6677	0.6389

K_{I0} is SIF at the tip of primary microcrack (1) when other microcracks were absent.

4. Discussion

This effort represents a study of fracture micromechanics of Haversian cortical bone through adoption of a simplified model. The simplifications were based on a number of fundamental assumptions. One such assumption has been the

adoption of LEFM. The application of this theory was based on the results of experimental efforts found in the literature. These results indicate that bone fracture follows linear elastic patterns [22–24]. Furthermore, Robertson et al. have reported that the plastic zone on the microcrack tips was approximately 1–5 μm, which was negligible in comparison to microcrack size [31]. The model also represents a plane strain condition. In long bone, longitudinal dimension is quite large in comparison to its diameter. The loading in the current model, occurs in a perpendicular direction to the longitudinal axis without altering the bone length. This leads to consideration of the plane strain condition in the two-dimensional model of cortical bone during lateral loading. The microcracks, in this paper, were assumed to be situated within the interstitial tissue. This point was also raised in the results of in vivo experiments [2,16]. Another factor is that a single osteon away from others is considered. Osteons are situated at close proximities in the real bone. The distance between the osteons and osteonal density will greatly influence the microcrack growth trajectory, thus affecting the fracture behavior of the bone. Detailed description of such a complex behavior requires that the stress intensity factor at the tip of individual microcracks be fully investigated. It is thus appropriate to place the emphasis on modeling a single osteon. Furthermore, consideration of an isolated osteon does not play a decisive factor as results have indicated that the effect of an osteon on fracture behavior is limited to the vicinity of the osteon. Articles published by Guo et al. confirm this approach [13].

It is also assumed that cement lines are not present. Here, stress fields at the microcrack tips are naturally affected by the existence of cement lines. Debonding phenomena and the corresponding osteon pull-out are the expected results of microcracks approaching the cement line boundary. This is primarily due to the weak interface between the cement line and the surrounding tissue. The material properties of the interfacing tissue are, however, not yet fully understood [15,16]. In addition, comparison of the osteon diameter of about 100 μm and cement line thickness which is close to 1–3 μm led to a decision to include the cement line in the future developments of the current model. In this study, microcracks are modeled before they reach the cement line. The results are therefore not greatly affected by the lack of cement line presence.

Another simplification was the exclusion of the Haversian channel in the model. The inclusion of the channel would have reduced the effective modulus of the osteon, thereby increasing the effect on the SIF at the microcrack tips. The placement of microcracks outside the osteon, however, did reduce the effect of Haversian channel exclusion upon microcrack fracture behavior. It could further be argued that if the microcrack reaches the Haversian channel by passing through the cement line boundary, fracture could occur due to the high stress concentration associated with this channel.

The results were a clear indication of the effect of microstructure heterogeneity upon Haversian cortical bone fracture behavior. It was shown that the osteonal effect upon microcracks changed as the mechanical properties of various microstructural tissues varied. These results were in accordance with other experimental and theoretical reports [12,13]. The effect of microstructure heterogeneity upon bone fracture behavior is primarily observed in the mechanical properties of tissues. Differences in mechanical properties of osteonal and interstitial tissues results in different deformations when the bone is subjected to an applied load. Localized stress concentrations could consequently occur at the interfaces [12]. This stress concentration affects the stress fields at the microcrack tips.

Experimental results indicate that the difference in mechanical properties associated with the osteons and interstitial tissues vary with age, disease, gender and genetic factors [18,32]. As an example, the bone remodeling associated with the aging process causes the secondary osteon to contain new bone in comparison to the interstitial region [12]. The mechanical properties of the osteon are expected to remain constant while the remodeling process during aging is sustained [12]. The properties associated with interstitial tissue, however, do not remain constant with aging [12]. This has a severe effect on the bone fracture mechanics. It could be argued that the underlying reason for an increased susceptibility of bone to fracture is due to changes in the mechanical properties of different tissues in the bone. It should also be added that the osteonal mechanical properties alter as the bone remodeling is retarded [13]. This also affects other phenomena such as the osteon pull-out. Osteon pull-out could also be affected by the existence of fluid in the bone. The effect of bone fluid upon fracture behavior at the microstructural level has not as yet been fully investigated. Comparison of the basic fracture experiments on wet and dry bones, however, indicate that osteon pull-out is slightly higher in the wet bone [22,23].

The results of this paper have shown that the effects of microcracks upon one another could lead to amplification or shielding of the stress intensity factor. This effect was, however, shown to be dependent upon the way microcracks were located with respect to each other. It could, therefore, be argued that fracture parameters were influenced by the interaction between microcracks. Other experimental results have also point to a direct relationship between microcracks and fracture behavior [33] in such a way that reduction of bone resistance to fracture has been found to be accompanied by the coalescence of microcracks [8,34].

In conclusion, the results of this paper emphasize the effect of microstructure morphology and heterogeneity upon fracture behavior. The provided mathematical formulation indicates that the stress field at the tip of the microcracks is greatly influenced by microstructure and the effect of existence of other microcracks. This could result in stress amplification or stress shielding. Further research towards providing a more detailed model through inclusion of the cement line debonding and osteon pull-out and the effect of microcracks on each others growth trajectories would be valuable.

Appendix A. Singular integral equations

The matrix consists of two edge dislocations with Burgers vectors b_x and b_y at the point s ($x_s = \xi$) on x axis (Fig. A.1). Stress for any point as $P(x, y)$ on the matrix could be determined as

$$\sigma_{xx} = k_{xx_1}(x, y, \xi)b_x + k_{xx_2}(x, y, \xi)b_y \tag{A.1a}$$

$$\sigma_{yy} = k_{yy_1}(x, y, \xi)b_x + k_{yy_2}(x, y, \xi)b_y \tag{A.1b}$$

$$\sigma_{xy} = k_{xy_1}(x, y, \xi)b_x + k_{xy_2}(x, y, \xi)b_y \tag{A.1c}$$

In Eq. (A.1) the variables are defined as

$$\begin{aligned} k_{xx_1}(x, y, \xi) = \frac{G_1}{\pi(k_1+1)R_0}\Bigg\{ & -2\left(1+\frac{2x_1^2}{r_1{}^2}\right)\frac{y_1R_0}{r_1{}^2} + \left(A+B+4A\frac{x_2^2}{r_2^2}\right)\frac{R_0y_2}{r_2^2} \\ & -2A\frac{\beta^2-1}{\beta^3}\left[2x_2 - 8\frac{x_2^3}{r_2^2} - \frac{\beta^2-1}{\beta}R_0\left(1-\frac{4x_2^2}{r_2^2}\right)\right]\frac{R_0^2y_2}{r_2^4} - \left(A+B+4A\frac{x^2}{r^2}\right)\frac{R_0y}{r^2} \\ & -(B-A)\frac{1}{\beta}\left(\frac{2xyR_0^2}{r^4}\right) - 2A\left(1-\frac{4x^2}{r^2}\right)\frac{R_0^3y}{r^4}\Bigg\} \end{aligned} \tag{A.2a}$$

$$\begin{aligned} k_{xx_2}(x, y, \xi) = \frac{G_1}{\pi(k_1+1)R_0}\Bigg\{ & -2\left(1-\frac{2x_1^2}{r_1^2}\right)\frac{x_1R_0}{r_1^2} + \left(A+B-4A\frac{x_2^2}{r_2^2}\right)\frac{R_0x_2}{r_2^2} \\ & +2A\frac{\beta^2-1}{\beta^3}\left[\beta^2\left(-1+\frac{2x_2^2}{r_2^2}\right) - \left(6\frac{x_2^2}{r_2^2} - \frac{8x_2^4}{r_2^4}\right) + \frac{\beta^2-1}{\beta}R_0\left(3-\frac{4x_2^2}{r_2^2}\right)\frac{x_2}{r_2^2}\right]\frac{R_0^2}{r^2} \\ & -\left(A+B-4A\frac{x^2}{r^2}\right)\frac{R_0x}{r^2} + [A(2\beta^2-1)+M(k_2+1)-1]\frac{1}{\beta}\left(1-\frac{2x^2}{r^2}\right)\frac{R_0^2}{r^2} + 2A\left(3-4\frac{x^2}{r^2}\right)\frac{R_0^3x}{r^4}\Bigg\} \end{aligned} \tag{A.2b}$$

$$\begin{aligned} k_{yy_1}(x, y, \xi) = \frac{G_1}{\pi(k_1+1)R_0}\Bigg\{ & -2\left(1-\frac{2x_1^2}{r_1^2}\right)\frac{y_1R_0}{r_1^2} + \left(3A-B-4A\frac{x_2^2}{r_2^2}\right)\frac{R_0y_2}{r_2^2} \\ & -2A\frac{\beta^2-1}{\beta^3}\left[-6x_2 + \frac{8x_2^3}{r_2^2} + \frac{\beta^2-1}{\beta}R_0\left(1-4\frac{x_2^2}{r_2^2}\right)\right]\frac{R_0^2y}{r_2^4} - \left(3A-B-4A\frac{x^2}{r^2}\right)\frac{R_0y}{r^2} \\ & +(B-A)\frac{1}{\beta}\left(\frac{2xyR_0^2}{r^4}\right) + 2A\left(1-4\frac{x^2}{r^2}\right)\frac{R_0^3y}{r^4}\Bigg\} \end{aligned} \tag{A.2c}$$

$$\begin{aligned} k_{yy_2}(x, y, \xi) = \frac{G_1}{\pi(k_1+1)R_0}\Bigg\{ & 2\left(3-\frac{2x_1^2}{r_1^2}\right)\frac{x_1R_0}{r_1^2} - \left(5A+B-4A\frac{x_2^2}{r_2^2}\right)\frac{R_0x_2}{r_2^2} \\ & -A\frac{\beta^2-1}{\beta^3}\left[2(2-\beta^2) - 4(5-\beta^2)\frac{x_2^2}{r_2^2} + \frac{16x_2^4}{r_2^4} + 2\frac{\beta^2-1}{\beta}\left(3-\frac{4x_2^2}{r_2^2}\right)\frac{R_0x_2}{r_2^2}\right]\frac{R_0^2}{r_2^2} \\ & +\left(5A+B-4A\frac{x^2}{r^2}\right)\frac{R_0x}{r^2} - [A(2\beta^2-1)+M(k_2+1)-1]\frac{1}{\beta}\left(1-\frac{2x^2}{r^2}\right)\frac{R_0^2}{r^2} - 2A\left(3-4\frac{x^2}{r^2}\right)\frac{R_0^3x}{r^4}\Bigg\} \end{aligned} \tag{A.2d}$$

$$k_{xy_1}(x,y,\xi)=\frac{G_1}{\pi(k_1+1)R_0}\left\{-2\left(1-\frac{2x_1^2}{r_1^2}\right)\frac{R_0x_1}{r_1^2}+\left(3A-B-4A\frac{x_2^2}{r_2^2}\right)\frac{R_0x_2}{r_2^2}\right.$$
$$-2A\frac{\beta^2-1}{\beta^3}\left[1-8\frac{x_2^2}{r_2^2}+8\frac{x_2^4}{r_2^4}+\frac{\beta^2-1}{\beta}\left(3-4\frac{x_2^2}{r_2^2}\right)\frac{R_0x_2}{r_2^2}\right]\frac{R_0^2}{r_2^2}-\left(3A-B-4A\frac{x^2}{r^2}\right)\frac{R_0x}{r^2}$$
$$\left.-(B-A)\frac{1}{\beta}\left(1-2\frac{x^2}{r^2}\right)\frac{R_0^2}{r^2}+2A\left(3-4\frac{x^2}{r^2}\right)\frac{R_0^3x}{r^4}\right\} \tag{A.2e}$$

$$k_{xy_2}(x,y,\xi)=\frac{G_1}{\pi(k_1+1)R_0}\left\{-2\left(1-\frac{2x_1^2}{r_1^2}\right)\frac{R_0y_1}{r_1^2}+\left(A+B-4A\frac{x_2^2}{r_2^2}\right)\frac{R_0y_2}{r_2^2}\right.$$
$$+2A\frac{\beta^2-1}{\beta^3}\left[2\beta^2x_2-4\left(x_2-2\frac{x_2^3}{r_2^2}\right)+\frac{\beta^2-1}{\beta}R_0\left(1-4\frac{x_2^2}{r_2^2}\right)\right]\frac{R_0^2y_2}{r_2^4}-\left(A+B-4A\frac{x^2}{r^2}\right)\frac{R_0y}{r^2}$$
$$\left.-[A(2\beta^2-1)+M(k_2+1)-1]\frac{2}{\beta}\frac{R_0xy}{r^4}+2A\left(1-4\frac{x^2}{r^2}\right)\frac{R_0^3y}{r^4}\right\} \tag{A.2f}$$

$$x_1=x-\xi,\qquad r_1^2=x_1^2+y^2 \tag{A.3a}$$

$$x_2=x-\frac{R_0^2}{\xi},\qquad r_2^2=x_2^2+y^2 \tag{A.3b}$$

$$r^2=x^2+y^2,\qquad \beta=\frac{\xi}{R_0} \tag{A.3c}$$

$$A=\frac{1-\mathrm{GR}}{1+\mathrm{GR}k_1} \tag{A.4a}$$

$$B=\frac{k_2-\mathrm{GR}k_1}{k_2+\mathrm{GR}} \tag{A.4b}$$

$$M=\frac{\mathrm{GR}(k_1+1)}{(k_2+\mathrm{GR})(k_2-1+2\mathrm{GR})} \tag{A.4c}$$

The resulting stress obtained through dislocation distribution b_t and b_n in the tangential and normal direction of microcracks could be expressed as

$$\sigma_{t_i}(t)=\sum_{j=1}^{n}\int_{-1}^{1}[k_{t_1}(s,t)b_t(s)+k_{t_2}(s,t)b_n(s)]\,\mathrm{d}s \tag{A.5a}$$

$$\sigma_{n_i}(t)=\sum_{j=1}^{n}\int_{-1}^{1}[k_{n_1}(s,t)b_t(s)+k_{n_2}(s,t)b_n(s)]\,\mathrm{d}s,$$
$$i,j=1,2,\ldots,n \tag{A.5b}$$

where

$$k_{t_1}=\left\{k_{xx_1}\left(\frac{-\sin(2\alpha_{ij})}{2}\right)+k_{yy_1}\left(\frac{\sin(2\alpha_{ij})}{2}\right)\right.$$
$$\left.+k_{xy_1}\cos(2\alpha_{ij})\right\}L_j \tag{A.6a}$$

$$k_{t_2}=\left\{k_{xx_2}\left(\frac{-\sin(2\alpha_{ij})}{2}\right)+k_{yy_2}\left(\frac{\sin(2\alpha_{ij})}{2}\right)\right.$$
$$\left.+k_{xy_2}\cos(2\alpha_{ij})\right\}L_j \tag{A.6b}$$

$$k_{n_1}=\{k_{xx_1}\sin^2(\alpha_{ij})+k_{yy_1}\cos^2(\alpha_{ij})-k_{xy_1}\sin(2\alpha_{ij})\}L_j \tag{A.6c}$$

$$k_{n_2}=\{k_{xx_2}\sin^2(\alpha_{ij})+k_{yy_2}\cos^2(\alpha_{ij})-k_{xy_2}\sin(2\alpha_{ij})\}L_j \tag{A.6d}$$

In Eq. (A6) α_{ij} could be defined as follow:

$$\alpha_{ij}=\alpha_j-\alpha_i \tag{A7}$$

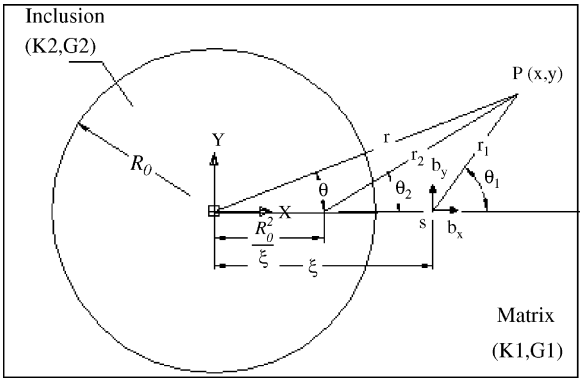

Fig. A.1. The edge dislocations b_x and b_y in the neighborhood of an inclusion.

Appendix B. Stress intensity factor (SIF) computation

The relationships between crack opening in different fracture modes (g_t, g_n) and the SIFs (K_I, K_{II}) could be expressed as

$$\frac{dg_n}{dr} = \frac{k+1}{2G}\frac{k_I}{\sqrt{2\pi r}} \tag{B.1a}$$

$$\frac{dg_t}{dr} = \frac{k+1}{2G}\frac{k_{II}}{\sqrt{2\pi r}} \tag{B.1b}$$

The relation between crack opening and dislocation density, on the other hand, could be described:

$$g_n(r) = \int_0^r B_n(r)\,dr \tag{B.2a}$$

$$g_t(r) = \int_o^r B_t(r)\,dr \tag{B.2b}$$

The resulting, SIFs (K_I, K_{II}) could thus be obtained by substituting Eq. (8) in Eqs. (B1) and (B2):

$$k_I|_{s=\pm1} = \pm\frac{2G_1}{k+1}\sqrt{L_i}\,f_n(\pm1) \tag{B.3a}$$

$$k_{II}|_{s=\pm1} = \pm\frac{2G_1}{k+1}\sqrt{L_i}\,f_t(\pm1) \tag{B.3b}$$

References

[1] Zioupos P, Currey JD. The extent of microcracking and the morphology of microcracks in damaged bone. J Mater Sci 1994;29:978–86.

[2] Burr DB, Stafford T. Validity of the bulk-staining technique to separate artifactual from in vivo microdamage. Clin Orthop Relat Res 1990;260:305–8.

[3] Martin RB. Mathematical model for repair of fatigue damage and stress fracture in osteonal bone. J Orthop Res 1995;13:309–16.

[4] Burr DB, Turner CH, Naick P, Forwood MR, Ambrosius W, Sayeed Hasan M, et al. Does microdamage accumulation affect the mechanical properties of bone? J Biomech 1998;31:337–45.

[5] Schaffler MB, Choi K, Milgrom C. Aging and matrix microdamage accumulation in human compact bone. Bone 1995;17:521–5.

[6] Forwood MR, Parker AW. Microdamage in response to repetitive tensional loading in the rat tibia. Calcif Tissue Int 1989;45:47–53.

[7] Norman TL, Wang Z. Microdamage of human cortical bone: incidence and morphology in long bones. Bone 1997;20(4):375–9.

[8] Yeni YN, Fyhrie DP. Fatigue damage-fracture mechanics interaction in cortical bone. Bone 2002;30(3):509–14.

[9] O'Brien FJ, Taylor D, Lee TC. The effect of bone microstructure on the initiation and growth of microcracks. J Orthop Res 2005;23:475–80.

[10] Burr DB, Forwood MR, Fyhrie DP, Martin RB, Schaffler MB, Turner CH. Bone microdamage and skeletal fragility in osteoporotic and stress fracture. J Bone Min Res 1997;12:6–15.

[11] Reily GC, Currey JD. The effects of damage and microcracking on the impact strength of bone. J Biomech 2000;33:337–43.

[12] Phelps JB, Hubbard GB, Wang X, Agrawal CM. Microsructural heterogeneity and the fracture toughness of bone. J Biomed Mater Res 2000;51:735–41.

[13] Guo XR, Liang LC, Goldstein SA. Micromechanics of osteonal cortical bone fracture. J Biomech Eng 1998;120:112–7.

[14] Fleck C, Eifler D. Deformation behavior and damage accumulation of cortical bone specimens from the equine tibia under cyclic loading. J Biomech 2003;36(2):179–89.

[15] Hogan HA. Micromechanics modeling of Haversian cortical bone properties. J Biomech 1992;25(5):549–56.

[16] Prendergast PJ, Huiskes R. Microdamage and osteocyte-lacuna strain in bone: a microstructural finite element analysis. J Biomech Eng 1996;118:240–6.

[17] Braidotti P, Branca FP, Sciubba E, Stagni L. An elastic compound tube model for a single osteon. J Biomech 1995;28(4):439–44.

[18] Doblaré M, García JM, Gómez MJ. Modeling bone tissue fracture and healing: a review. Eng Fract Mech 2004;71(13/14):1809–40.

[19] Simmons ED, Pitzker KPH, Grynpas MD. Age-related changes in the human femoral cortex. J Orthop Res 1991;9:155–67.

[20] Nalla RK, Kruzic JJ, Kinney JH, Ritchie RO. Effect of aging on the toughness of human cortical bone: evaluation by R-curves. Bone 2004;35(6):1240–6.

[21] Erdogan F, Gupta GD, Ratwani M. Interaction between a circular inclusion and an arbitrarily oriented crack. J Appl Mech 1974:1007–13.

[22] Bonfield W. Advances in the fracture of cortical bone. J Biomech 1987;20(11/12):1071–81.

[23] Melvin JM. Fracture mechanics of bone. J Biomech Eng 1993;115:549–54.

[24] Behiri JC, Bonfield W. Fracture mechanics of bone—the effects of density, specimen thickness and crack velocity on longitudinal fracture. J Biomech 1984;17(1):25–34.

[25] Lakes RS, Nakamura S, Behiri JC, Bonfield W. Fracture mechanics of bone with short cracks. J Biomech 1990;23(10):967–75.

[26] Akkus O, Rimnac CM. Cortical bone tissue resists fatigue fracture by deceleration and arrest of microcrack growth. J Biomech 2001;34:757–64.

[27] Martin RB, Burr DB. Stress distribution on the Haversian canal due to microcracks in a cortical bone. J Biomech 1982;15:137–9.

[28] Zysset PK, Guo XE, Hoffler CE, Moore KE, Goldstein SA. Elastic modulus and hardness of cortical and trabecular bone lamellae measured by nonoindentation in the human femur. J Biomech 1999;32:1005–12.

[29] Goodier JN. Concentration of stress around spherical and cylindrical inclusions and flaws. Appl Mech 1932;55:39–44.

[30] Dundurs J, Mura T. Interaction between an edge dislocation and a circular inclusion. J Mech Phys Solids 1964;12:177–89.

[31] Robertson DM, Robertson D, Barrett CR. Fracture toughness, critical crack length and plastic zone size in bone. J Biomech 1978;11:359–64.

[32] Crofts RD, Boyce TM, Bloebaum RD. Aging changes in osteon mineralization in the human femoral neck. Bone 1994;15:137–52.

[33] Courtney AC, Hayes WC, Gibson LJ. Age-related differences in post-yield damage in human cortical bone: experiment and model. J Biomech 1996;29(11):1463–71.

[34] Boyce TM, Fyhrie DP, Glotkowski MC, Radin EL, Schaffler MB. Damage type and strain mode association in human compact bone bending fatigue. J Orthop Res 1998;16:322–9.